International Symposium
On Turbulence and Shear Flow
Phenomena (TSFP-9)
June 30 - July 3, 2015 *Melbourne, Australia*

AN EDQNM MODEL FOR MODERATELY ANISOTROPIC TURBULENT FLOWS IN TERMS OF SPHERICALLY-AVERAGED DESCRIPTORS

Vincent Mons
Institut Jean Le Rond d'Alembert
UPMC Univ Paris 06 and CNRS, UMR 7190
Paris, F-75005, France
vincent.mons@sfr.fr

Pierre Sagaut
M2P2 Laboratory
UMR CNRS 7340
Aix-Marseille Université
IMT La Jetée, Technopole de Château-Gombert
38, rue Frédéric Joliot-Curie
13451 Marseille Cedex 13, France
pierre.sagaut@uni-amu.fr

Claude Cambon
Laboratoire de Mécanique des Fluides et d'Acoustique
École Centrale de Lyon and CNRS, UMR 5509
Écully, F-69131, France
claude.cambon@ec-lyon.fr

INTRODUCTION

In this paper, a new system of governing equations for spherically-averaged descriptors is derived for predicting incompressible homogeneous turbulent flows in the presence of arbitrary mean velocity gradients. First, the equations governing the second-order spectral tensor $\hat{R}_{ij}(\boldsymbol{k},t)$ are closed with the Eddy-Damped Quasi-Normal Markovian (EDQNM) approximation. Then, a representation of $\hat{R}_{ij}(\boldsymbol{k},t)$ in terms of spherically-averaged descriptors is injected in its closed governing equations, and the latter are integrated analytically over spheres of radius $k=\|\boldsymbol{k}\|$. This procedure allows to circumvent the practical difficulties that arise from the $\boldsymbol{k}$ dependence of $\hat{R}_{ij}(\boldsymbol{k},t)$. A remarkable feature of this model is that it makes a disctinction between directional anisotropy and polarization anisotropy, which are treated separately. Spherical averaging allows to obtain a model for anisotropic turbulence that is as versatile as the classical EDQNM model for isotropic turbulence, i.e. this model can calculate anisotropic turbulent flows at both very high and low Reynolds numbers, with good resolution of both large and small scales and over very long evolution times. However, spherical integration entails a loss of information, and the upper boundary of anisotropy intensity that can be investigated with the present model is derived from realizability conditions.

Several flow configurations are considered to assess the validity of the present model. A satisfactory agreement with experiments of grid-generated turbulence subjected to successive plane strains is observed, which confirms the capability of the model to account for production of anisotropy by mean flow gradients. The case of homogeneous turbulence subjected to a constant pure plane shear is also investigated. In addition to recovering typical spectral slopes for energy and cross-correlation spectra, the subtle interplay between linear and nonlinear effects is reproduced, yielding the eventual exponential growth of the turbulent kinetic energy.

CLOSED EQUATIONS FOR $\hat{R}_{ij}(\boldsymbol{k},t)$

The present model is derived starting from the governing equation for the second-ordrer spectral tensor $\hat{R}_{ij}(\boldsymbol{k},t)$, which is the Fourier transform of the two-point second-order correlation tensor $R_{ij}(\boldsymbol{r},t)=\langle u_i(\boldsymbol{x},t)u_j(\boldsymbol{x}+\boldsymbol{r},t)\rangle$, where $u_i(\boldsymbol{x},t)$ is the fluctuating velocity field, $\boldsymbol{r}$ the vector separating the two points in physical space, and the operator $\langle\rangle$ denotes ensemble average. Starting from a trace-deviator splitting of $\hat{R}_{ij}(\boldsymbol{k},t)$ restricted to the plane normal to the wave vector $\boldsymbol{k}$ by virtue of incompressibility, it can be shown (Cambon & Jacquin, 1989) that this tensor is generated from scalar spectra according to:

$$\hat{R}_{ij}(\boldsymbol{k},t)=\mathscr{E}(\boldsymbol{k},t)P_{ij}(\boldsymbol{k})+\Re\left(Z(\boldsymbol{k},t)N_i(\boldsymbol{k})N_j(\boldsymbol{k})\right) \qquad (1)$$

$\mathscr{E}(\boldsymbol{k},t)$ is the energy density in 3D Fourier space, the difference between $\mathscr{E}(\boldsymbol{k},t)$ and its spherical average allows to quantify directional anisotropy, whereas $Z(\boldsymbol{k},t)$ characterizes polarization anisotropy, or tensorial anisotropy at a given wave vector. $P_{ij}(\boldsymbol{k})$ denotes the projection operator onto the plan perpenticular to $\boldsymbol{k}$ and $N_i(\boldsymbol{k})$ refers to the helical modes (Sagaut & Cambon, 2008). By virtue of this decomposition, the governing equation for $\hat{R}_{ij}(\boldsymbol{k},t)$ is equivalent to a set of two equations in terms of the scalars $\mathscr{E}(\boldsymbol{k},t)$ and $Z(\boldsymbol{k},t)$:

$$\left(\frac{\partial}{\partial t}-\lambda_{In}k_l\frac{\partial}{\partial k_n}+2\nu k^2\right)\mathscr{E}(\boldsymbol{k},t)-\mathscr{E}(\boldsymbol{k},t)S_{ij}\alpha_i\alpha_j \\ +\Re\left(Z(\boldsymbol{k},t)S_{ij}N_iN_j\right)=T^{(\mathscr{E})}(\boldsymbol{k},t) \qquad (2)$$

$$\left(\frac{\partial}{\partial t}-\lambda_{ln}k_l\frac{\partial}{\partial k_n}+2\nu k^2\right)Z(\boldsymbol{k},t)-Z(\boldsymbol{k},t)S_{ij}\alpha_i\alpha_j$$
$$+\mathscr{E}(\boldsymbol{k},t)S_{ij}N_i^*N_j^*-2\mathrm{i}Z(\boldsymbol{k},t)\left(\frac{W_l}{2}\alpha_l-\Omega_E\right)=T^{(Z)}(\boldsymbol{k},t) \tag{3}$$

where $N_i=N_i(\boldsymbol{k})$, $\alpha_i=k_i/k$, S_{ij} is the symmetric part of the mean velocity gradient λ_{ij}, which is space uniform, and W_i is linked to its antisymmetric part. The generalized Lin equations (2)-(3) also involve the nonlinear transfer terms $T^{(\mathscr{E})}(\boldsymbol{k},t)$ and $T^{(Z)}(\boldsymbol{k},t)$, which are expressed in terms of a third-order spectral tensor. The expressions of $T^{(\mathscr{E})}(\boldsymbol{k},t)$ and $T^{(Z)}(\boldsymbol{k},t)$ are closed and written in terms of the scalars $\mathscr{E}(\boldsymbol{k},t)$ and $Z(\boldsymbol{k},t)$ via an EDQNM approximation, which states that the fluctuating velocity probability distributions are not too far from normal distributions (Millionschikov, 1941). Thus, the governing equations for third-order correlations can be closed. The departure from normal law is taken into account via an eddy-damping term that allows to preserve realizability (Orszag, 1970). As a complementary assumption, the proper memory of triple correlations is truncated via a Markovianization procedure in order to simplify their closed expressions. Since turbulent flows interacting with mean velocity gradients leading to kinetic energy production are considered in the present work, the simplest EDQNM version, where explicit effects induced by mean gradient are discarded in the expressions of third-order correlations, is employed here. This is in constrast with previous EDQNM models dealing with turbulent flows dominated by interacting dispersive waves (Cambon & Jacquin, 1989).

GOVERNING EQUATIONS FOR SPHERICALLY-AVERAGED DESCRIPTORS

Even closed, the $\boldsymbol{k}$ dependence of $\mathscr{E}(\boldsymbol{k},t)$ and $Z(\boldsymbol{k},t)$ makes equations (2)-(3) difficult to be solved from a practical point of view. The expressions of the nonlinear tranfer terms $T^{(\mathscr{E})}(\boldsymbol{k},t)$ and $T^{(Z)}(\boldsymbol{k},t)$ closed by the EDQNM approximation involve integrals over the 3D Fourier space that are coslty to evaluate. In order to circumvent these difficulties, one solution is to integrate analytically the closed Lin equations (2)-(3) over spheres of radius $k=\|\boldsymbol{k}\|$. This analytical integration requires a representation of the tensor $\hat{R}_{ij}(\boldsymbol{k},t)$. Here, we choose the representation of Cambon & Rubinstein (2006) which is written in terms of $\mathscr{E}(\boldsymbol{k},t)$ and $Z(\boldsymbol{k},t)$ as:

$$\mathscr{E}(\boldsymbol{k},t)=\frac{E(k,t)}{4\pi k^2}\left(1-15H_{ij}^{(dir)}(k,t)\alpha_i\alpha_j\right) \tag{4}$$
$$Z(\boldsymbol{k},t)=\frac{5}{2}\frac{E(k,t)}{4\pi k^2}H_{ij}^{(pol)}(k,t)N_i^*(\boldsymbol{k})N_j^*(\boldsymbol{k}) \tag{5}$$

Equations (4)-(5) involve the tensors $H_{ij}^{(dir)}(k,t)$ and $H_{ij}^{(pol)}(k,t)$ that depend only on k and measure respectively directional anisotropy and polarization anisotropy according to:

$$2E(k,t)H_{ij}^{(dir)}(k,t)=\iint_{S_k}\hat{R}_{ij}^{(dir)}(\boldsymbol{k},t)\mathrm{d}^2\boldsymbol{k} \tag{6}$$
$$2E(k,t)H_{ij}^{(pol)}(k,t)=\iint_{S_k}\hat{R}_{ij}^{(pol)}(\boldsymbol{k},t)\mathrm{d}^2\boldsymbol{k} \tag{7}$$

where $\hat{R}_{ij}^{(dir)}(\boldsymbol{k},t)$ and $\hat{R}_{ij}^{(pol)}(\boldsymbol{k},t)$ refer respectively to the directional and polarization parts of $\hat{R}_{ij}(\boldsymbol{k},t)$. $E(k,t)$ is the kinetic energy spectrum and $\iint_{S_k}\mathrm{d}^2\boldsymbol{k}$ denotes integration over a spherical shell of radius k. Injecting this representation into equations (2)-(3) allows to integrate analytically the latter over spheres of radius k and to derive a system of equations in terms of the spherically-averaged descriptors $E(k,t)$, $H_{ij}^{(dir)}(k,t)$ and $H_{ij}^{(pol)}(k,t)$. The latter completely determine the second-order spectral tensor $\hat{R}_{ij}(\boldsymbol{k},t)$ according to (4)-(5). The resulting system is of the form:

$$\left(\frac{\partial}{\partial t}+2\nu k^2\right)E(k,t)=\mathscr{S}^L(k,t)+T(k,t) \tag{8}$$
$$\left(\frac{\partial}{\partial t}+2\nu k^2\right)E(k,t)H_{ij}^{(dir)}(k,t)=\mathscr{S}_{ij}^{L(dir)}(k,t)+\mathscr{S}_{ij}^{NL(dir)}(k,t) \tag{9}$$
$$\left(\frac{\partial}{\partial t}+2\nu k^2\right)E(k,t)H_{ij}^{(pol)}(k,t)=\mathscr{S}_{ij}^{L(pol)}(k,t)+\mathscr{S}_{ij}^{NL(pol)}(k,t) \tag{10}$$

The tensors $\mathscr{S}^L(k,t)$, $\mathscr{S}_{ij}^{L(dir)}(k,t)$ and $\mathscr{S}_{ij}^{L(pol)}(k,t)$ account for the interactions with the mean flow and are derived from the linear terms in (2)-(3), whereas $T(k,t)$, $\mathscr{S}_{ij}^{NL(dir)}(k,t)$ and $\mathscr{S}_{ij}^{NL(pol)}(k,t)$ correspond to nonlinear transfer terms and are derived from the expressions of $T^{(\mathscr{E})}(\boldsymbol{k},t)$ and $T^{(Z)}(\boldsymbol{k},t)$ closed by the EDQNM approximation. The expressions of these tensors can be found in Mons *et al.* (2015).

Spherical averaging allows to significantly reduce the computational cost, but also implies a loss of information. It can be shown that the representation (4)-(5) corresponds to the first-order truncation of expansions of the scalars $\mathscr{E}(\boldsymbol{k},t)$ and $Z(\boldsymbol{k},t)$ in terms of spherical harmonics (Cambon & Rubinstein, 2006). The degree of anisotropy permitted by the representation (4)-(5) is derived from the realizability condition $\mathscr{E}(\boldsymbol{k},t)\geqslant 0\,\forall\boldsymbol{k},t$, which is equivalent to:

$$\max_i\Lambda_i\left(\mathsf{H}^{(dir)}(k,t)\right)\leq\frac{1}{15}\,\forall k,t \tag{11}$$

where $\Lambda_i\left(\mathsf{H}^{(dir)}(k,t)\right)$ refers to the eigenvalues of $H_{ij}^{(dir)}(k,t)$.

COMPARISON WITH THE EXPERIMENTS OF GENCE AND MATHIEU

In the experiments of Gence & Mathieu (1979, 1980), a plane strain is first applied to quasi-isotropic grid-turbulence. A second strain is then applied whose principal axes have been rotated an angle α in the plane of the first strain. The mean-velocity gradients corresponding to the first and second strains are, respectively:

$$\lambda=\begin{pmatrix}0&0&0\\0&S&0\\0&0&-S\end{pmatrix},\quad \lambda=\begin{pmatrix}0&0&0\\0&S\cos(2\alpha)&-S\sin(2\alpha)\\0&-S\sin(2\alpha)&-S\cos(2\alpha)\end{pmatrix} \tag{12}$$

In Gence & Mathieu (1980), the original experimental device is extended in such a way that the turbulence can develop downstream without a mean-velocity gradient.

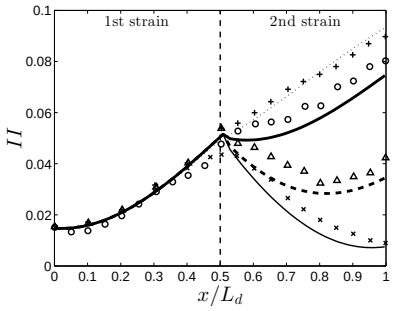

(a)

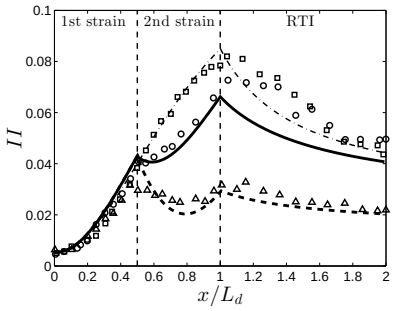

(b)

Figure 1: Evolution of the invariant II versus the position in the distorting duct of length L_d for the experiments of (a) Gence & Mathieu (1979) and (b) Gence & Mathieu (1980). Symbols correspond to experimental data and lines are obtained with the system of governing equations (8)-(10). Various values of the angle α between the principal axes of the two successive plane strains are investigated: $\alpha = 0$ ($\square$, - - -), $\alpha = \frac{\pi}{8}$ (+, ·····), $\alpha = \frac{\pi}{4}$ ($\circ$, ——), $\alpha = \frac{3\pi}{8}$ ($\triangle$, - -) and $\alpha = \frac{\pi}{2}$ ($\times$, ——).

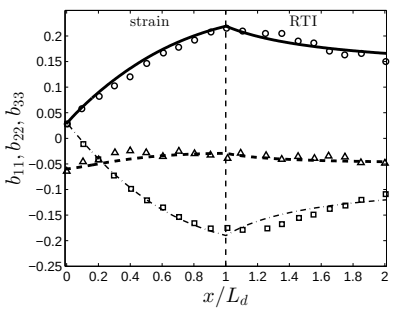

(a)

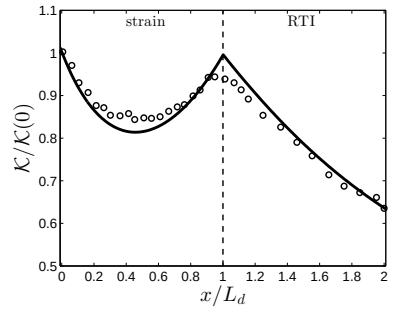

(b)

Figure 2: Evolution of (a) the anisotropy indicators b_{11} ($\triangle$, - -), b_{22} ($\square$, - · - ·) and b_{33} ($\circ$, ——) and (b) that of the turbulent kinetic energy $\mathscr{K}$ ($\circ$, ——) versus the position in the distorting duct of length L_d for the experiment in Gence & Mathieu (1980) without rotation in the second part of the distorting duct ($\alpha = 0$). Symbols correspond to experimental data and lines are obtained with the system of governing equations (8)-(10).

For these experiments, $S \simeq 2.9\tau_0^{-1}$ with $\tau_0 = \mathscr{K}(0)/\varepsilon(0)$. $\mathscr{K}(t)$ and $\varepsilon(t)$ refer to the turbulent kinetic energy and the dissipation rate respectively, and the origin corresponds to the entrance of the distorting duct. The simulations are initialized with a Taylor microscale-based Reynolds number of $Re_\lambda = 60$. Experimental data for the downstream evolution of the invariant II defined by:

$$II(t) = b_{ij}(t)b_{ji}(t), \quad b_{ij}(t) = \frac{\langle u_i u_j \rangle(t)}{2\mathscr{K}(t)} - \frac{\delta_{ij}}{3} \qquad (13)$$

are reported in figure 1 along with numerical results obtained with the system of governing equations (8)-(10). This figure shows a good agreement between experimental and numerical results, especially taking into account the uncertainty in the initial condition and a possible homogeneity fault in the experimental device. The system of governing equations (8)-(10) allows to correctly capture the evolution of anisotropy, both in the straining regions and during the relaxation phases. Only the period of return to isotropy (RTI) for the angle $\alpha = \frac{\pi}{4}$ is not fully satisfactory, mainly because the boundary between the straining and relaxation regions in the experiments does not appear to be as clear as in the simulations. The case of straining without rotation in the second part of the distorting duct ($\alpha = 0$), followed by a relaxation phase, is further illustrated in figure 2. The present model properly captures the evolution of the anisotropy indicators b_{ij} and that of the turbulent kinetic energy, both in the region dominated by linear effects and in the purely nonlinear one.

TURBULENCE SUBJECTED TO A STRAINING-RELAXATION-DESTRAINING CYCLE

The present model is further tested by comparing its predictions with the experiment of Chen *et al.* (2006), where a piston is used to apply plane straining and destraining on turbulence generated by active grids. The mean-velocity gradient in the experiment is of the form

$$\lambda(t) = \begin{pmatrix} S(t) & 0 & 0 \\ 0 & -S(t) & 0 \\ 0 & 0 & 0 \end{pmatrix} \qquad (14)$$

where the temporal evolution of $S(t)$ is given by figure 3(a). Initially, the mean flow corresponds to plane straining ($S(t) > 0$), until $t/\tau_0 \simeq 0.5$. After a relaxation phase ($0.5 \leq t/\tau_0 \leq 0.7$), destraining ($S(t) < 0$) is applied to the turbulence. In this experiment, the Reynolds number at the begining of the straining cycle is $Re_\lambda \simeq 400$. The maximum value of the strain $S(t)$ reached in the experiment is $\simeq 9.5\tau_0^{-1}$. Figure 3(b) illustrates the temporal evolution of

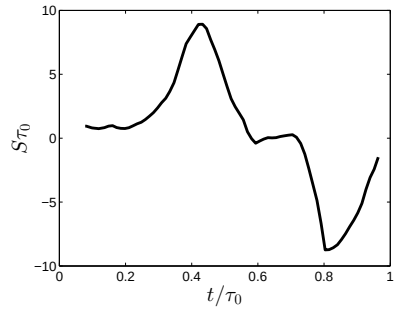

(a)

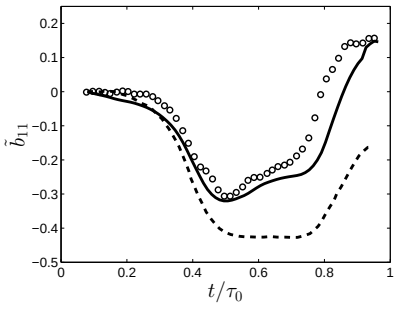

(b)

Figure 3: (a) Temporal evolution of the strain $S(t)$ applied to the turbulence; (b) experimental values ($\circ$), numerical values obtained with the present model (▬▬) and RDT prediction (▪▪) for the temporal evolution of the anisotropy indicator $\tilde{b}_{11}(t)$ in the experiment of Chen *et al.* (2006).

the anisotropy indicator $\tilde{b}_{11}(t)$, a two-component surrogate of the anisotropic tensor $b_{ij}(t)$. Experimental and numerical values obtained with the present model are reported, along with the Rapid Distortion Theory (RDT) prediction, provided by Chen *et al.* (2006), corresponding to the mean flow defined by equation (14) and figure 3(a). The temporal evolution of $\tilde{b}_{11}(t)$ shows good agreement between the experiment and the present model. From the comparison with RDT results, it appears that nonlinear phenomena are significant on a quantitative level. This is partly due to the presence of a relaxation phase in the straining cycle. Thus, the validity of both linear and nonlinear contributions in the system of governing equations (8)-(10) can be confirmed by the comparison with this experiment.

HOMOGENEOUS SHEAR TURBULENCE

Finally, we address the case of homogeneous turbulence subjected to a constant, maintained mean shear. The corresponding mean-velocity gradient is given by:

$$\lambda = \begin{pmatrix} 0 & 0 & S \\ 0 & 0 & 0 \\ 0 & 0 & 0 \end{pmatrix} \qquad (15)$$

The simulation is initialized with $Re_\lambda = 50$, the shear rate is fixed at $S = 2\tau_0^{-1}$, and the turbulence is initially isotropic. The temporal evolutions of the components of the deviatoric tensor $b_{ij}(t)$ and that of the kinetic energy $\mathscr{K}(t)$ are reported in figure 4. Such an exponential growth of the kinetic energy (figure 4(b)), which originates from nonlinear energy redistributions (RDT predicts a linear growth for $\mathscr{K}(t)$), is consistent with theoretical predictions (Tavoularis, 1985). Concerning results in spectral space, the kinetic energy spectrum $E(k,t)$ at $St = 50$ (figure 5(a)) displays a well-defined $-5/3$ slope in the inertial range as reported in experiments or DNS. Figure 5(b) reports the cross-correlation spectrum $\varphi_{13}(k,t)$ at $St = 50$. The latter evolves like $k^{-\frac{7}{3}}$ in the inertial range as predicted theoretically and observed in experiments and DNS (Ishihara *et al.*, 2002). This result, along with the exponential growth of the kinetic energy, supports the validity of the nonlinear contributions in the present model in the case of homogeneous shear turbulence.

CONCLUSION

A new model to calculate moderatly anisotropic flows has been derived in the present study. Remarkable features of this model are that it makes a distinction between directional anisotropy and polarization anisotropy, which are treated separately, and that no heuristic tuning of arbitrary constants is required. Analytical spherical averaging allows a significant reduction in the computational cost compared to other spectral models in 3D Fourier space. The EDQNM approximation is employed for the closure of the nonlinear transfer terms.

A satisfactory agreement with the experiments of Gence & Mathieu (1979, 1980) has been observed, which confirms the capability of the model to account for production of anisotropy by mean flow gradients. The relaxation phases in these experiments are also correclty captured, which supports the validity of the nonlinear tranfer terms. In addition, the model fits well the recent experiment with straining-relaxaxion-destraining (Chen *et al.*, 2006). For turbulence continuously subjected to a pure plane shear, the model ensures a correct asymptotic regime with constant values for the components of the dimensionless deviatoric tensor $b_{ij}(t)$ associated to the Reynolds stress tensor. The exponential growth of the turbulent kinetic energy mediated by nonlinear pressure redistribution terms is reproduced. Both $-5/3$ and $-7/3$ power laws are recovered for the spherically averaged energy spectrum and its non-diagonal component

REFERENCES

Cambon, C. & Jacquin, L. 1989 Spectral approach to non-isotropic turbulence subjected to rotation. *Journal of Fluid Mechanics* **202**, 295–317.

Cambon, C., Mansour, N. N. & Godeferd, F. S. 1997 Energy transfer in rotating turbulence. *Journal of Fluid Mechanics* **337**, 303–332.

Cambon, C. & Rubinstein, R. 2006 Anisotropic developments for homogeneous shear flows. *Physics of Fluids* **18**, 085106.

Chen, J., Meneveau, C. & Katz, J. 2006 Scale interactions of turbulence subjected to a straining-relaxation-destraining cycle. *Journal of Fluid Mechanics* **562**, 123 – 150.

Gence, J. N. & Mathieu, J. 1979 On the application of successive plane strains to grid-generated turbulence. *Journal of Fluid Mechanics* **93**, 501–513.

Gence, J. N. & Mathieu, J. 1980 The return to isotropy of an homogeneous turbulence having been submitted to two successive plane strains. *Journal of Fluid Mechanics* **101**, 555–566.

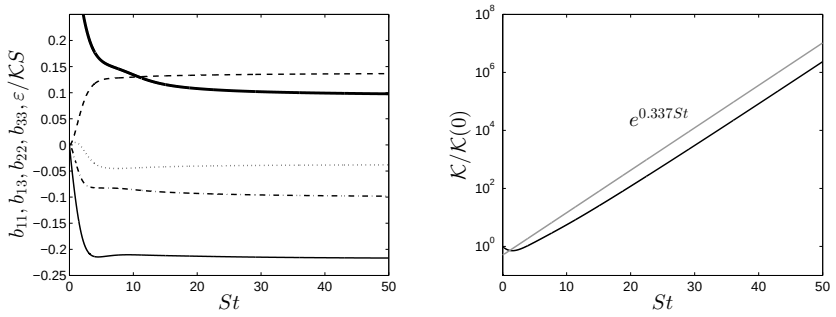

(a) (b)

Figure 4: Temporal evolutions of (a) the different components of the global anisotropy tensor $b_{ij}(t)$ and the ratio $\frac{\varepsilon}{S\mathscr{K}}$ (b_{11}, b_{13}, b_{22}, b_{33} and $\frac{\varepsilon}{S\mathscr{K}}$) and (b) that of the turbulent kinetic energy $\mathscr{K}(t)$ (black line) for homogeneous shear turbulence.

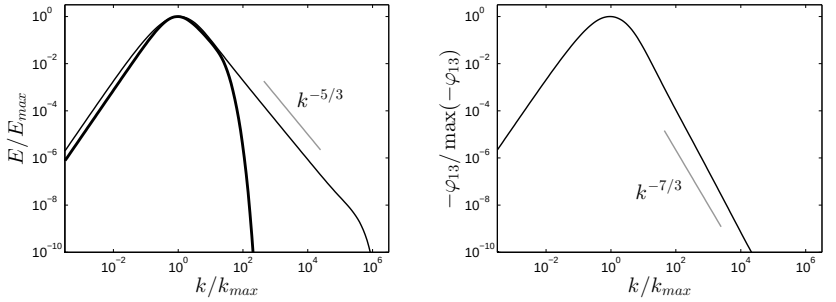

(a) (b)

Figure 5: (a) Energy spectrum $E(k,t)$ and (b) cross-correlation spectrum $\varphi_{13}(k,t)$ at $St = 0$ (thick black line) and $St = 50$ (thin black lines).

Ishihara, T., Yoshida, K. & Kaneda, Y. 2002 Anisotropic Velocity Correlation Spectrum at Small Scales in a Homogeneous Turbulent Shear Flow . *Physical Review Letters* **88**, 154501, 1–4.

Millionschikov, M. D. 1941 Theory of homogeneous isotropic turbulence. *Doklady Akademii nauk SSSR* **33**, 22–24.

Mons, V., Cambon, C. & Sagaut, P. 2015 Scale-by-scale modelling of anisotropic turbulence: effect of mean shear and return-to-isotropy. *Journal of Fluid Mechanics* **submitted for publication**.

Orszag, S. A. 1970 Analytical theories of turbulence. *Journal of Fluid Mechanics* **41**, 363 – 386.

Sagaut, P. & Cambon, C. 2008 *Homogenous Turbulence Dynamics*. Cambridge University Press.

Tavoularis, S. 1985 Asymptotic laws for transversely homogeneous turbulent shear flows. *Physics of Fluids* **28**, 999–1001.